Langmuir

Article

pubs.acs.org/Langmuir

Specific Ion Effects on the Self-Assembly of Ionic Surfactants: A Molecular Thermodynamic Theory of Micellization with Dispersion Forces

Boris Lukanov[†] and Abbas Firoozabadi*[,‡]

[†]Reservoir Engineering Research Institute, 595 Lytton Avenue, Suite B, Palo Alto, California 94301, United States

[‡]Department of Chemical Engineering, Yale University, New Haven, Connecticut 06511, United States

Supporting Information

ABSTRACT: The self-assembly of amphiphilic molecules is a key process in numerous biological and chemical systems. When salts are present, the formation and properties of molecular aggregates can be altered dramatically by the specific types of ions in the electrolyte solution. We present a molecular thermodynamic model for the micellization of ionic surfactants that incorporates quantum dispersion forces to account for specific ion effects explicitly through ionic polarizabilities and sizes. We assume that counterions are distributed in the diffuse region according to a modified Poisson−Boltzmann equation and can reach all the way to the micelle surface of charge. Stern layers of steric exclusion or distances of closest approach are not imposed externally; these are accounted for through the counterion radial distribution profiles due to the incorporation of dispersion potentials, resulting in a simple and straightforward treatment. There are no adjustable or fitted parameters in the model, which allows for a priori quantitative prediction of surfactant aggregation behavior based only on the initial composition of the system and the surfactant molecular structure. The theory is validated by accurately predicting the critical micelle concentration (CMC) for the well-studied sodium dodecyl sulfate (SDS) surfactant and its alkaline-counterion derivatives in mono- and divalent salts, as well as the molecular structure parameters of SDS micelles such as aggregation numbers and micelle surface potential.

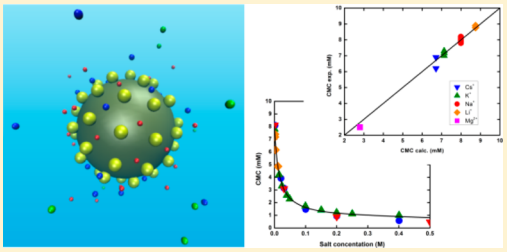

I. INTRODUCTION

Specific ion effects are ubiquitous in chemistry and biology. They occur in bulk solutions, where the solubility of comparable mono- and divalent salts can differ by orders of magnitude, and at interfaces, where the surface tension can vary considerably. Salts affect the stability of proteins,[1,2] play a major role in atmospheric and ocean chemistry,[3,4] influence the interaction between colloid particles,[5] and affect the aggregation of amphiphilic molecules such as surfactants.[6] Surfactants find countless applications in modern society, ranging from household products such as pharmaceuticals, foods, paints, detergents, and cosmetics to industrial processes involving coatings and lubricants (e.g., enhanced oil recovery) as well as applications in the emerging fields of nanotechnology and nanomedicine. The numerous practical uses of surfactants stem from the intrinsic duality in their molecular structure; they contain a hydrophobic tail that can be a hydrocarbon, fluorocarbon, siloxane, or polymer and a hydrophilic headgroup that can be ionic or nonionic (polar). This variety in the structure of surfactants allows for extensive variation in their behavior in solutions, in microemulsions, and at interfaces. As a result, a detailed understanding of the link among salt effects, surfactant molecular structure and solution physicochemical properties is essential to discovering novel applications or improving the efficiency of existing surfactant-based processes. At the same time, given the numerous household and industrial pathways through which surfactants enter the environment, a deeper understanding of the structure and aggregation behavior of these materials can help us design and synthesize them with minimal environmental impact.

Ionic surfactants with hydrocarbon tails are the most widely used class of surfactants in both industrial applications and academic research. When ionic surfactants are dissolved in electrolyte solutions, an increase in the solution ionic strength leads to a significant lowering of the critical micelle concentration (CMC) at which they start to aggregate. The lowering of the CMC can be attributed to the incorporation of salt counterions into the micelle surface, where they screen the electrostatic repulsions between the charged ionic surfactant headgroups, as well as to the effect of ions on the interfacial tension, dielectric constant, and density of the electrolyte solution. Micelle surfaces are porous, nonuniform, fluctuating entities, a feature that can allow for the accumulation of counterions between surfactant headgroups. A self-consistent field lattice model study of ionic surfactant micelles[7] and molecular dynamics simulations of anionic sodium dodecyl

Received: March 20, 2014
Revised: May 11, 2014
Published: May 15, 2014

dx.doi.org/10.1021/la501008x | *Langmuir* 2014, 30, 6373−6383

sulfate micelles[8−10] indeed indicates that a significant fraction of the counterions released by surfactant heads may accumulate between them, effectively reducing the charge in the interfacial region. A sound molecular thermodynamic model of micellization should therefore allow for the presence of micelle-bound counterions intercalated between the headgroups on the micelle surface.

The specific counterion type can have a similarly strong effect on the micellar properties, even when the counterions are of the same valence. For anionic dodecyl sulfates, for example, the CMC follows the Hofmeister (lyotropic) series as the alkali counterion size is increased: $CMC_{Li^+} > CMC_{Na^+} > CMC_{K^+} > CMC_{Cs^+}$.[11] This phenomenon cannot be explained by classical electrolyte theories such as the Derjaguin−Landau−Verwey−Overbeek (DLVO) theory of colloids or the Onsager−Samaras (OS) interface theory, which do not distinguish between different 1:1 salt solutions. The Hofmeister effect was first observed more than 100 years ago,[12] yet it has remained an enigma for over a century. Only recently have more cogent analytical approaches to explaining ion specificity started to emerge in the scientific literature.[13]

One approach is based on Collins's concept of matching water affinities.[14] Depending on how they interact with water, ions can be divided into two main groups: kosmotropes and chaotropes (Figure 1). Kosmotropes are smaller, have a higher

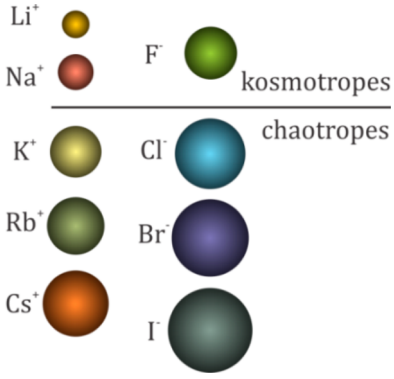

Figure 1. Group IA alkali cations and group VIIA halide anions divided into kosmotropes (strongly hydrated) and chaotropes (weakly hydrated) according to their size.[14] The ions are drawn approximately to the scale of their bare radii.[15]

charge density and a lower polarizability, and interact strongly with the water dipole. This creates a hydration shell around the ion with water dipoles pointing toward or away from it, depending on the ion type (cation or anion, Figure 2a,b). Chaotropes, in contrast, are larger, with low charge density and high electrostatic polarizability. They interact weakly with water, and the water molecules form a stronger hydrogen bond network (cage) around the ion, much like they do around nonpolar solutes (Figure 2c).[16] When a salt contains two small kosmotropes (like NaF), strong electrostatic interactions keep the two ions close together (Figure 2d).[17] In a salt containing two large chaotropes (like CsBr), the ions still remain close together even though they interact weakly because the water molecules prefer to form a stronger hydrogen bond network around them (Figure 2e). However, a salt having one small and one large ion, such as NaBr, is very soluble in water because the small ion prefers to solvate water molecules than to interact with the large ion. The two ions remain separated, with intact hydration shells as in Figure 2f. The picture outlined above can

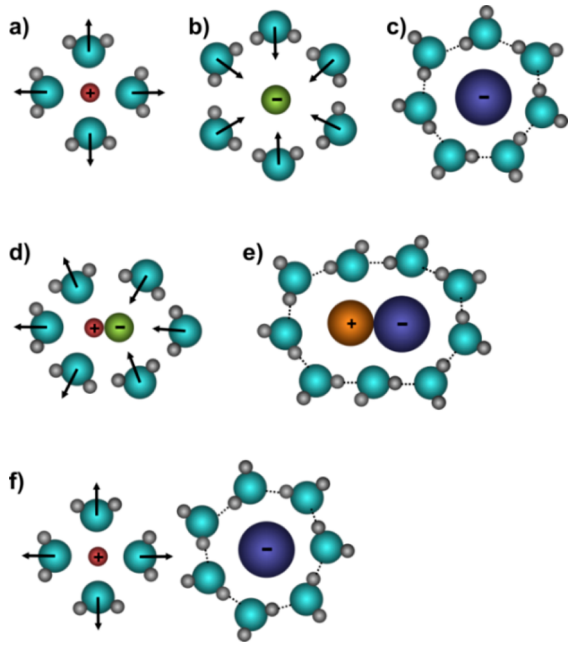

Figure 2. Specific ion interactions and salt solubilities in water. (a) Water's dipole points away from a kosmotrope cation. (b) Water's dipole points toward a kosmotrope anion. (c) Hydrogen bonding around a chaotrope anion. (d) Water structure around two kosmotrope ions. (e) Hydrogen-bond cage around two chaotrope ions. (f) Separation (dissolution) of a kosmotrope−chaotrope pair. The black arrows indicate water dipoles.

be quantified in theoretical models by incorporating various ionic hydrated sizes, degrees of hydration shell overlap, and distances of closest approach between different ions.[17]

A more analytical approach to ion specificity has been developed by Ninham and collaborators in a series of papers published over the past decade and a half.[18−21] They demonstrate that the proper inclusion of quantum mechanical nonelectrostatic dispersion interactions missing from the classical theories of electrolytes can account for ion-specific effects at surfaces and in colloidal suspensions. Dispersion interactions involve the frequency-dependent dynamic polarizabilities of the ions and include the van der Waals induced dipole−induced dipole dispersion (London) forces between the ions and the interface. The dispersion forces can be extracted from extensions of the Lifshitz theory[22] and are highly ion-specific. It seems that in a consistent and predictive molecular thermodynamic theory these forces should be integrated at the same level as "normal" electrostatic interactions in order to account for specific ion effects fully.

Despite considerable progress in the study of micellar solutions and the extensive experimental data in the literature, there are few molecular thermodynamic theories of micellization that assess the role of ion specificity and counterion binding in the aggregation of ionic surfactants. Nagarajan and Ruckenstein[23] neglected counterion binding onto the micelle surface and assumed the released counterions to be distributed in the electrical diffuse layer surrounding the micelles as described by the Poisson−Boltzmann (PB) equation. In the classical Poisson−Boltzmann formulation, dispersion potentials are disregarded and all ions are treated as point charges with no physical volume, a priori ignoring any ion-specific effects. Srinivasan and Blankschtein[24,25] allowed for counterion binding onto the micelle surface, but ion-specific effects were still largely

dx.doi.org/10.1021/la501008x | Langmuir 2014, 30, 6373−6383

ignored; the only effect considered was the hydrated size of the counterions adsorbed onto the micelle surface. In an earlier model,[26] we adopted Srinivasan and Blankschtein's idea of counterion binding onto the micelle surface and made an attempt to quantify ion-specific effects by incorporating Collins's concept of matching water affinities. This was achieved through a somewhat ad hoc approach involving various Stern layers, headgroup−counterion hydration shell overlap, and contact distances. These parameters are not easily accessible through experiments and are essentially adjustable to fit the experimental data.

In this article, we put the theoretical treatment of ion-specific effects in micellization on more solid analytical footing by incorporating dispersion forces in the framework of a more generalized Poisson−Boltzmann (PB) theory. We will see that ion specificity emerges naturally from the calculations and specific-ion effects are adequately implemented through ionic polarizability and size only, without the need for externally fitted unknowns such as Stern layers, headgroup−counterion contact-pair overlap estimates, and so forth. These constraints are naturally accounted for via dispersion interactions. In this sense, the model is simple and predictive; all parameters are obtained from experimental data or from first principles calculations available in the literature. Another theory of micellization with dispersion forces has recently been published by Koroleva and Victorov.[27] As in our earlier model, the authors employ various ionic distances of closest approach, which are adjusted to match experimental data. Moreover, the dispersion coefficients and salting-out (Setschenow) constants for different ions are not calculated explicitly, effectively increasing the number of fitted parameters. In the model we present here, these parameters are fixed (either calculated explicitly or adopted from the literature) and therefore nonadjustable.

Our results successfully reproduce the ion-specific variations of the CMC of alkyl dodecyl sulfates in both mono- and divalent salts and are in better agreement with experiment than previous theories. The model also provides a detailed glimpse into the molecular structure of ionic micelles by delivering information on variables such as micelle aggregation number, degree of counterion binding, counterion radial density distribution, and micelle surface potential. These results also reveal significant ion-specific variations that replicate the lyotropic series and follow the trends established in experimental studies.

II. THERMODYNAMICS OF MICELLIZATION

A. Model Basics. We consider a multicomponent system with a fixed composition of water, surfactant, and electrolyte. The total numbers of molecules of each are N_W, N_S, and N_{salt}, respectively, where the latter is the number of ionic pairs of added inorganic salt. The temperature T and pressure p for the system are fixed. Thus, there are five fixed parameters that characterize the system: N_W, N_S, N_{salt}, T, and p.

The Gibbs free energy of the system can be expressed as

$$G = G_f + G_m + G_i \tag{1}$$

where G_f is the free energy of formation, G_m is the energy of mixing, and G_i is the free energy of interaction between the species. We assume a dilute solution and no micelle interactions. Thus, G_i can be neglected, and

$$G = G_f + G_m \tag{2}$$

Let us analyze each of the two energy contributions on the right-hand side of eq 2 separately. The first, the free energy of formation G_f, can be written as the sum of the formation energies for each of the various system components. The components are water molecules, monodisperse (nonaggregated) surfactant molecules, micelles (composed of surfactant molecules and micelle-bound ions), and free ions in the solution:

$$G_f = N_W\mu_W^\circ(T, p) + N_{1S}\mu_{1S}^*(T, p) + \sum_{g=2}^{\infty} N_g\mu_g^*(T, p) + \sum_i N_i^{free}\mu_i^*(T, p) \tag{3}$$

where we have introduced several new variables: N_{1S} is the number of monodisperse surfactant molecules; N_g is the number of micelles of size g (with g being the number of surfactant molecules in the micelle); N_i^{free} is the number of free ions of species i in the solution; $\mu_W^\circ(T, p)$, $\mu_{1S}^*(T, p)$, $\mu_g^*(T, p)$, and $\mu_i^*(T, p)$ are the respective chemical potentials, where the superscript $^\circ$ signifies the standard-state chemical potential for a pure substance and * signifies infinite dilution. N_{1S}, N_g, and N_i^{free} can be defined from the following material balance equations:

$$N_S = N_{1S} + gN_g \tag{4a}$$

$$N_i = N_i^{free} + g\beta_i N_g \text{ for } i = 1,\ 2,\ 3,\ 4,\ \ldots \tag{4b}$$

Here N_i is the total number of ions of species i in the system (free + micelle-bound), and β_i is the degree of counterion binding of species i, i.e., the fraction that represents the average number of bound counterions of species i per surfactant molecule in the micelle.[24]

N_i can be calculated from the valence of the various species and from the total number of added ion pairs N_{salt}. Let z_S be the valence of the surfactant ionic head, let z_1 be the valence of the counterion if the surfactant head is anionic, and let z_2 be the valence of the counterion if the surfactant head is cationic. The surfactant headgroups are assumed to be fully dissociated, i.e., every counterion is released in the solution. Then

$$N_1 = \left|\frac{z_S}{z_1}\right| N_S \text{ and } N_2 = 0 \tag{5a}$$

when the surfactant is anionic ($z_S < 0$) and

$$N_1 = 0 \text{ and } N_2 = \left|\frac{z_S}{z_2}\right| N_S \tag{5b}$$

when the surfactant is cationic ($z_S > 0$).

If one type of salt is added to the solution, then we will have salt ions in the solution besides the surfactant counterions. Let z_3 and z_4 be the valences of the cation and anion of the added salt. Assuming that the salt is fully dissociated,

$$N_3 = |z_4|N_{salt} \tag{5c}$$

$$N_4 = |z_3|N_{salt} \tag{5d}$$

Additional salts can be added to the solution in a similar manner. Note that all N_i depend only on the fixed variables N_S and N_{salt}.

We assume that the micelles are monodisperse. This assumption is known as the maximum term approximation

dx.doi.org/10.1021/la501008x | Langmuir 2014, 30, 6373−6383

and is based on the recognition that for spherical and globular micelles the size distribution is usually very narrow; hence, the concentration of aggregates other than that corresponding to the maximum in the size distribution is assumed to be small.[28] With this assumption, we eliminate the summation sign in eq 3, and the formation free energy becomes

$$G_f = N_W\mu_W^\circ + N_{1S}\mu_{1S}^* + N_g\mu_g^* + \sum_i N_i^{free}\mu_i^* \quad (6)$$

By substituting mass balance eqs 4a and 4b into eq 6,

$$G_f = N_W\mu_W^\circ + (N_S - gN_g)\mu_{1S}^* + N_g\mu_g^* + \sum_i (N_i - g\beta_i N_g)\mu_i^* \quad (7)$$

and reorganizing,

$$G_f = N_W\mu_W^\circ + N_S\mu_{1S}^* + N_g\mu_g^* - gN_g\mu_{1S}^* - \sum_i g\beta_i N_g\mu_i^* + \sum_i N_i\mu_i^* \quad (8)$$

or

$$G_f = N_W\mu_W^\circ + N_S\mu_{1S}^* + N_g g\Delta\mu_g^* + \sum_i N_i\mu_i^* \quad (9)$$

Here, we have defined $\Delta\mu_g^* = (\mu_g^* - g\mu_{1S}^* - \sum_i g\beta_i\mu_i^*)/g$ as the free energy of micellization per surfactant molecule in the micelle. It is the difference in the standard-state chemical potentials between a surfactant molecule in an aggregate containing g surfactant molecules and $\sum_i g\beta_i$ adsorbed counterions and singly dispersed surfactants and single ions dissolved in water. The various contributions to the free energy of micellization will be discussed in a separate section below.

Next, we define the expression for the free energy of mixing G_m. Assuming an ideal solution (no enthalpy of mixing, negligible interactions), the free energy of mixing is simply the entropy of mixing × T:

$$G_m = kT[N_W \ln X_W + N_{1S} \ln X_{1S} + N_g \ln X_g + \sum_i N_i^{free} \ln X_i^{free}] \quad (10)$$

where k is the Boltzmann constant and X_l is the mole fraction of the species l:

$$X_l = \frac{N_l}{N_W + N_{1S} + N_g + \sum_i N_i^{free}} \quad (11)$$

for l = W, 1S, g, $i(i = 1, 2, 3, 4...)$

Combining eq 1 with eqs 9 and 10, we obtain the expression for the total Gibbs free energy of the system:

$$G = G_f + G_m = N_W\mu_W^\circ + N_S\mu_{1S}^* + N_g g\Delta\mu_g^* + \sum_i N_i\mu_i^* + kT[N_W \ln X_W + N_{1S} \ln X_{1S} + N_g \ln X_g + \sum_i N_i^{free} \ln X_i^{free}] \quad (12)$$

Since some of the terms in the expression above depend only on the fixed variables, we can subtract those terms and define G' as

$$G' = G - N_W\mu_W^\circ - N_S\mu_{1S}^* - \sum_i N_i\mu_i^* = gN_g\Delta\mu_g^* + kT[N_W \ln X_W + N_{1S} \ln X_{1S} + N_g \ln X_g + \sum_i N_i^{free} \ln X_i^{free}] \quad (13)$$

Dividing by kT provides the final expression for the Gibbs free energy:

$$\frac{G'}{kT} = \frac{gN_g\Delta\mu_g^*}{kT} + N_W \ln X_W + N_{1S} \ln X_{1S} + N_g \ln X_g + \sum_i N_i^{free} \ln X_i^{free} \quad (14)$$

To find the minimum of the total Gibbs free energy, eq 14 is minimized with respect to the independent variables g, N_g, and β_i subject to the material balance constraints (eqs 4a and 4b) under the maximum term approximation. g and N_g appear in eq 14 explicitly, while β_i appears implicitly through the term $\Delta\mu_g^*$. Minimization is executed using the FSQP algorithm,[29] and the result of the minimization is compared to the equivalent expression for the system without micellization:

$$\frac{G'}{kT} = N_W \ln X_W + N_{1S} \ln X_{1S} + \sum_i N_i^{free} \ln X_i^{free} \quad (15)$$

The minimum of the total Gibbs free energy is determined by the lower of the two values and is the necessary and sufficient condition for chemical equilibrium. In the literature, the equality of chemical potentials is often used as the condition for chemical equilibrium. While the equality of chemical potentials is a necessary condition for equilibrium, it is not always a sufficient one as it does not ensure the global minimum of the Gibbs free energy.

B. Micellar Structure and Solution Properties. We make several important assumptions about the micellar interface structure, the effects of counterion binding, and the solution properties near the micelle surface. A schematic representation of our model is shown in Figure 3. For spherical micelles, the radius of the hydrocarbon core is labeled R_c. The center of charge of the surfactant heads lies on a surface of radius $R_{ch} = R_c + d_{ch}$ referred to as the micellar surface of charge. The surfactant heads, surfactant, and salt counterions and salt co-ions are assumed to be spherical, and their radii are obtained from ref 30.

In contrast to earlier models, we do not artificially impose various Stern layers at the micelle−water interface and counterions are allowed to reach all the way to the micelle surface of charge. We believe that this is a reasonable assumption, given that micelle surfaces, unlike solid surfaces, are porous, nonuniform, fluctuating entities that can allow for the accumulation of counterions between the surfactant heads. As mentioned in the Introduction, several studies have indicated that a significant fraction of the counterions released by surfactant heads accumulate between them, effectively reducing the charge in the interfacial region.[7−10] Similar to Srinivasan and Blankschtein, we assume that a fraction of the counterions are adsorbed (bound) at the micelle surface of charge. As such, they are expected to reduce the Gibbs free energy of the micelle−electrolyte interface formation by shielding parts of the interface, to participate in steric repulsions, and to contribute to the headgroup−counterion entropy of mixing at the interface. The fraction of adsorbed ions per surfactant molecule for each of the counterion species

dx.doi.org/10.1021/la501008x | Langmuir 2014, 30, 6373−6383

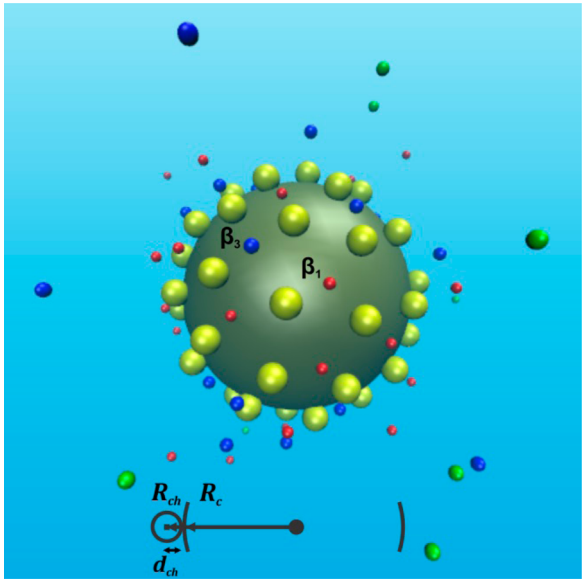

Figure 3. Three-dimensional schematic representation of a micelle with the diffuse region around it. R_c is the radius of the hydrocarbon core. d_{ch} is the distance to the micelle surface of charge where the headgroups and bound counterions are located. Color scheme: headgroups (yellow), headgroup counterions (red), salt counterions (blue), salt coins (green). The size of ions of the same color may appear different due to the 3D perspective.

is determined by the respective degree of counterion binding β_i. In Figure 3, the two types of adsorbed counterions are thus labeled β_1 and β_3, in accordance with eqs 5a and 5c. The surfactant heads and the bound counterions are assumed to be arranged randomly on the micelle surface of charge and any discreteness of the g surfactant heads and the $g\beta_i$ bound counterions is neglected, resulting in a surface of uniform charge density. Srinivasan and Blankschtein carefully evaluated the importance of discrete ion charges at the interface and concluded that neglecting discreteness does not significantly alter the physics of counterion binding since the high degree of screening from the diffuse ion cloud reduces the net self-potential of each discrete ion at the interface.[24]

The counterions remaining in the bulk solution assemble to form the diffuse ion cloud around the micelle. In the diffuse layer, we incorporate ion dispersion forces within the Poisson–Boltzmann theoretical framework of Coulombic interactions. Dispersion potentials depend on both the ionic size and ionic polarizability, as will be shown below. Moreover, we will see that the incorporation of dispersion forces significantly affects the counterion radial density profiles around the micelle. Ion-specific properties emerge naturally from these profiles. As a result, the counterion distances of closest approach related to the ions' kosmotropic or chaotropic attributes are automatically accounted for through the dispersion potentials without the need for externally imposed Stern layer estimates.

C. Free Energy of Micellization. The most important term in our expression for the total Gibbs free energy of the system (eq 14) and one which we have not yet discussed is the free energy of micellization $\Delta\mu_g^*$. This free-energy change associated with the formation of the surfactant aggregate (i.e., the energy change in forming a micelle from singly dispersed surfactants molecules) can be expressed as the sum of six free-energy contributions that are calculated from the chemical structure of the various micellar components (surfactant molecules, ions) and the solution properties:[23,24,26]

$$\Delta\mu_g^* = (\Delta\mu_g^*)_{\text{transf}} + (\Delta\mu_g^*)_{\text{deform}} + (\Delta\mu_g^*)_{\text{interface}} + (\Delta\mu_g^*)_{\text{steric}} + (\Delta\mu_g^*)_{\text{entropic}} + (\Delta\mu_g^*)_{\text{ionic}} \quad (16)$$

The first three terms are related to the formation of the micellar core, which is assumed to be like a liquid hydrocarbon. These terms account for the transfer of the surfactant tail from the solution to the hydrocarbon core, deformation of the tail within the core, and formation of the hydrocarbon–solution interface. The last three terms account for the formation of the micelle–water interfacial shell where the ionic headgroups and counterions reside. Explicit expressions for the first five terms in eq 16 have appeared in the literature,[23,24,26] and we will not discuss them here. (For the sake of completeness, we provide detailed expressions and derivations in the SI.) Instead, we focus on the last term of eq 16, which embodies our most significant departure from previous theories.

D. Ionic Free Energy $(\Delta\mu_g^*)_{\text{ionic}}$ and Dispersion Potentials. We evaluate the ionic free energy of micelle formation based on the structure of the micelle interfacial shell as depicted in Figure 3. The ionic free energy of the micelle surface and double layer around it is equal to the amount of work performed in building up the charged surface and the double layer around the micelle by a reversible and isothermal process. It is given by the Guntelberg charging process:[31,32]

$$\frac{(\Delta\mu_g^*)_{\text{ionic}}}{kT} = \frac{a_{\text{ch}}}{kT}\int_0^{\sigma} \phi_0(\sigma')\, \mathrm{d}\sigma' \quad (17)$$

Here, σ is the final surface charge density at the micelle surface of charge per surfactant molecule, ϕ_0 is the electrical potential at the micelle surface of charge per surfactant molecule, and a_{ch} is the area per surfactant molecule at the micelle surface of charge:

$$a_{\text{ch}} = \frac{4\pi R_{\text{ch}}^{\,2}}{g} \quad (18)$$

The integration variable σ' in eq 17 is the instantaneous surface charge density which varies from 0 to σ as the surface is charged. The trapezoidal rule is used for the numerical integration of eq 17. The final charge density σ is given by

$$\sigma = \frac{e[z_S + \sum_i z_i\beta_i]}{a_{\text{ch}}} \quad (19)$$

The electrical potential at the micelle surface ϕ_0 in eq 17 is generally determined by solving the Poisson–Boltzmann (PB) equation in spherical coordinates

$$\frac{\mathrm{d}^2\phi}{\mathrm{d}r^2} + \frac{2}{r}\frac{\mathrm{d}\phi}{\mathrm{d}r} = -\frac{e}{\epsilon_0\epsilon_{\text{sol}}}\sum_i z_i n_i^{\infty} \exp\left\{-\frac{[z_i e\phi(r)]}{kT}\right\} \quad (20)$$

where $n_i^{\infty} = 10^3 N_{\text{Avogadro}} C_i^{\infty}$ is the ionic concentration at $r = \infty$. Equation 20 is a second-order differential equation that we solve numerically (using finite differences) with two boundary conditions. The first is that the potential vanishes at infinity:

$$\lim_{r\to\infty} \phi = 0$$
$$\lim_{r\to\infty} \nabla\phi = 0 \quad (21)$$

dx.doi.org/10.1021/la501008x | Langmuir 2014, 30, 6373–6383

The second is the electric field at the surface of charge:

$$\nabla\phi|_{r=R_{ch}} = -\frac{\sigma}{\epsilon_0\epsilon_{sol}} \tag{22}$$

We have already discussed some of the severe limitations of eq 20 in which ions are effectively considered to be point charges interacting only through Coulombic forces with the micelle surface (ionic valence is the only relevant factor). The missing quantum fluctuation (dispersion) forces in the PB formulation clearly play a significant role in ion-specific effects and ion/surface hydration. Thus, in a consistent and predictive theory, dispersion effects will have to be included at the same level as the nonlinear electrostatic forces that form the skeletal framework of the classical theory.

In several recent theoretical papers, Ninham and co-workers have generalized the Poisson−Boltzmann theory to account for ion properties such as the ionic polarizability and hydrated size.[18,19,21] They have shown that ions of different polarizability experience significantly different dispersion interactions with a charged surface, which can induce up to a 2-fold change in the electrostatic surface potential compared to that predicted by classical electrolyte theory. The effects considered by Ninham et al. underline the central role of ionic polarizabilities and ion sizes. Here, we follow their approach to account for ion-specific dispersion effects.

The relative equivalence between electrostatic and dispersion forces is established by taking the interaction potential between ions i and the micelle surface to equal

$$U_i(r) = U_i^{electrostatic}(r) + U_i^{dispersion}(r) \tag{23}$$

where the electrostatic part is simply $U_i^{electrostatic} = z_i e\phi(r)$ as in the exponent in eq 20 and $U_i^{dispersion}(r)$ describes the nonelectrostatic dispersion energy of an ion a distance r from an interface. By adding the dispersion term, the generalized PB (eq 20) becomes

$$\frac{d^2\phi}{dr^2} + \frac{2}{r}\frac{d\phi}{dr} = -\frac{e}{\epsilon_0\epsilon_{sol}} \sum_i z_i n_i^{\infty} \exp\left\{-\frac{[z_i e\phi(r) + U_i^{dispersion}(r)]}{kT}\right\} \tag{24}$$

The exact form of the dispersion potential can be extracted from Lifshitz theory[33,34] and has an r^{-3} form,

$$U_i^{dispersion}(r) = \frac{B_i}{r^3}h_i(r) \tag{25}$$

where

$$h_i(r) = 1 + \frac{2r}{\sqrt{\pi}\,a_i}\left[\frac{2r^2}{a_i^2} - 1\right]\exp\left(-\frac{r^2}{a_i^2}\right) - \left[1 + \frac{4r^4}{a_i^4}\right]\mathrm{erfc}\left(\frac{r}{a_i}\right) \tag{26}$$

is a form factor that accounts for the finite size of the ion and a_i is the Gaussian radius of the ion based on the assumption that the radial dependence of the polarizability of the electron cloud around a molecule can be approximated by a Gaussian function.[34,35] The ionic size is thus included in the calculations, taking us beyond the limitations of point-charge models. For a point ion, $h_i(r) \equiv 1$, and for an ion sufficiently far from the interface, $h_i(r) \approx 1$, whereas the dispersion energy at contact with a surface reaches a finite limit such that $U_i^{dispersion}(r = 0) = 16B_i/3\pi^{1/2}a_i^3$.[34]

The dispersion coefficients B_i can be determined from the dynamic polarizability $\alpha_i(i\omega)$ of the ion and include dipolar contributions from all electromagnetic frequencies. They can be positive (repulsive potential) or negative (attractive potential), depending on the solvent, surface, and ion properties (dielectric functions, polarizabilities, and ionic sizes). More precisely, the dispersion coefficients are determined from the effective excess polarizability $\alpha_i^*(i\omega)$, which accounts for the depolarization effects of the solvent, modulated at all frequencies by the difference in the dielectric functions $\varepsilon_{hc}(i\omega)$ of the surface (hydrocarbon) and $\varepsilon_W(i\omega)$ of the solvent (water)[21]

$$B_i = \frac{kT}{4}\sum_{n=0}^{\infty}(2 - \delta_{0,n})\frac{\alpha_i^*(i\omega_n)\Delta(i\omega_n)}{\varepsilon_w(i\omega_n)} \tag{27}$$

where

$$\Delta(i\omega_n) = \frac{\varepsilon_w(i\omega_n) - \varepsilon_{hc}(i\omega_n)}{\varepsilon_w(i\omega_n) + \varepsilon_{hc}(i\omega_n)} \tag{28}$$

is the difference in the dielectric responses of the micelle surface and the solvent. The summation in eq 27 is over imaginary quantized oscillator frequencies $i\omega_n$, where $\omega_n = 2\pi nkT/\hbar$. The $(2 - \delta_{0,n})$ factor indicates that the $n = 0$ term is taken with a factor of 1/2 compared to the other terms in the summation.

By treating the ion as a dielectric sphere with a Gaussian volume V_i, Landau and Lifshitz have deduced an expression for the ionic effective polarizability[34,36]

$$\alpha_i^*(i\omega_n) = \frac{3V_i}{4\pi}\frac{[\varepsilon_i(i\omega_n) - \varepsilon_w(i\omega_n)]}{[\varepsilon_i(i\omega_n) + 2\varepsilon_w(i\omega_n)]} \tag{29}$$

with the dielectric function of the ion derived from its intrinsic dynamic polarizability in vacuum $\alpha_i(i\omega_n)$:

$$\varepsilon_i(i\omega_n) = 1 + 4\pi\frac{\alpha_i(i\omega_n)}{V_i} \tag{30}$$

The dynamic polarizability, in turn, can be decomposed into a series of electronic transitions each characterized by frequency ω_j with oscillator strength f_j multiplied by the ion's intrinsic static polarizability α_0:[34]

$$\alpha_i(i\omega_n) = \alpha_{0,i}\sum_j \frac{f_{j,i}}{1 + \frac{\omega_n^2}{\omega_{j,i}^2}} \tag{31}$$

Thus, to calculate the effective ionic polarizability $\alpha_i^*(i\omega_n)$ we need the values of f_j, ω_j, α_0, and V for each ionic species i. We use the values obtained by Parsons and Ninham, who used ab initio calculations with coupled cluster single and double (CCSD) excitation-level theory and density functional theory (DFT) to obtain f_j, ω_j, α_0 and, similarly, ab initio calculations at a Hartree−Fock (HF) level of theory to obtain the ionic Gaussian volumes and radii V_i and a_i.[30,34] For kosmotropic ions, we use the hydrated radii as suggested by the authors.

We plot our calculated values for the effective ionic polarizabilities versus angular frequency for several monovalent cations (Figure 4a) and anions (Figure 4b). We notice that the effective polarizabilities of ions in water vary according to the Hofmeister series and in fact appear negative for kosmotropic ions (Li^+, Na^+, and F^-) and positive for chaotropic ions (K^+, Cs^+, Cl^-, Br^-, and I^-) (cf. Figure 1). It thus seems that ion-specific properties emerge naturally from the above equations.

dx.doi.org/10.1021/la501008x | Langmuir 2014, 30, 6373−6383

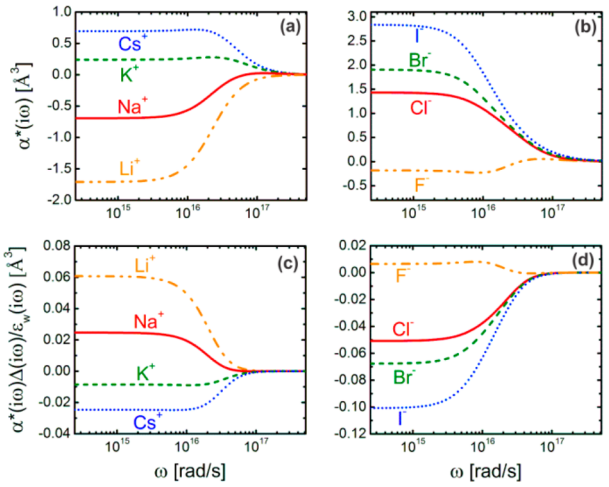

Figure 4. Excess polarizability of cations (a) and anions (b) in water. Frequency summand for the interaction energy between the water–hydrocarbon interface and cations (c) or anions (d). Shown from ω_1 to ω_n for $n = 2100$ in the frequency summation. The lower limit of the frequency range is given by the first nonzero frequency, which at room temperature is 2.14×10^{14} rad/s.

This is a very powerful result. Conventionally, ions are divided into kosmotropes and chaotropes based on the empirical Jones–Dole viscosity coefficients, which are essentially a measure of the ion–water interaction strength.[14] The viscosity coefficients happen to be positive for some ions (kosmotropes) and negative for others (chaotropes). We see that the same distinction emerges naturally from the equations above, now a result of an analytic theory rather than an empirical observation.

In order to calculate the summands in eq 27 and the dispersion coefficients B_i, we also need to know the frequency-dependent dielectric functions of the solvent and the micelle surface. For a molecule with one characteristic absorption frequency (the ionization frequency ω_I), the dielectric function can be approximated by a simple one-oscillator model:[21,37,38]

$$\varepsilon(i\omega_n) = 1 + \frac{n^2 - 1}{1 + \frac{\omega_n^2}{\omega_I^2}} \tag{32}$$

For the refractive indices of water and dodecane, we use the values $n_W = 1.333$ and $n_{hc} = 1.42$, respectively, and for the characteristic absorption frequencies, we use $\omega_{I,w} = 2\pi(h\nu_{I,w})/h$ where $h\nu_{I,w} = 2.0 \times 10^{-11}$ erg and $\omega_{I,hc} = 1.9 \times 10^{16}$ [rad/s].[37,39] We plot the frequency summand of eq 27 in Figure 4c for cations and 4d for anions.

We can see that the summand is positive for kosmotropic ions and negative for chaotropic ions. The dispersion coefficients are now straightforward to calculate (eq 27) and are listed in Table 1. We see that they too are positive for kosmotropes, resulting in a repulsive potential with the chaotropic hydrocarbon–water micelle interface, and negative for chaotropes, resulting in an attractive potential with the chaotropic micelle surface. Interestingly, these values reflect Collins' concept of matching affinities: the like ion/surface pairs are attracted to each other and the dissimilar ion/surface pairs are repelled from one other. Thus, the chaotrope–kosmotrope interactions discussed in the Introduction emerge naturally from the treatment above in a simple and straightforward fashion. We will see that they are also reflected in the ion radial density profiles around the micelle and that the distances of closest approach can be extracted from the profiles.

Table 1. Calculated Dispersion Coefficients for Several Monovalent Cations and Anions with a Hydrocarbon–Water Interface

cation	Li^+	Na^+	K^+	Cs^+
B [10^{-50} J m^3]	1.16	0.398	−0.34	−0.79
anion	F^-	Cl^-	Br^-	I^-
B [10^{-50} J m^3]	0.102	−0.98	−1.16	−1.58

III. RESULTS AND DISCUSSION

A. Critical Micelle Concentration of Alkyl Dodecyl Sulfates. We now transition to the validation of our model by applying it to one of the most widely studied and used surfactants, sodium dodecyl sulfate (SDS), and its counterion derivatives, alkyl dodecyl sulfates. We use a value of 25 Å^2 for the cross-sectional area of the sulfate headgroup[24] and a value of $d_{ch} = 3.5$ Å for the distance from the micelle core to the surface of charge (one sulfate radius plus half a C–O bond length). The critical micelle concentration (CMC) is the most important characteristic of surfactant systems and the one most accurately determined in experiments. We calculate it by minimizing the Gibbs free energy of the system for different values of N_S and construct a plot of the monodisperse surfactant concentration X_{1S} versus the total surfactant concentration $X_S = X_{1S} + gX_g$. The plot is marked by a sharp change in the slope as the concentration reaches the CMC. Similarly, the experimentally measured physical properties of the solution such as surface tension, electrical conductivity, and light-scattering intensity exhibit a sharp change at the onset of micellization. The experimental values for the CMC obtained by these different methods are usually close to one another, although not necessarily identical.[40]

We first investigate the role of the specific counterion in the CMC of dodecyl sulfates. In Figure 5a, we plot the calculated CMC of Li^+, Na^+, K^+, Cs^+, and Mg^{2+} dodecyl sulfates versus the experimental data obtained from various sources and techniques. Ideally, all points should fall on the diagonal line. As evident, the agreement between predicted and experimental values is very good, both in terms of the trend (Hofmeister series) and the quantitative values. In fact, our values are in significantly better agreement with experiment compared to our previous model[26] (to the best of our knowledge, the only model to study counterion specificity in dodecyl sulfates), even though we have no adjustable or fitted parameters. The multiple points along the vertical (experimental) axis are due to discrepancies between the different experimental studies. For example, the experimentally determined CMC of SDS may vary from 7.6 to 8.3 mM at 25 °C.

To evaluate the effect of increasing salt concentration, we calculate the variation of the CMC of SDS in NaCl (Figure 5b). The correspondence with experimental data is excellent throughout the salt concentration range, and the observed lowering of the CMC is accurately reproduced. The agreement is better than in any of the previous models.[23,24,26,27] In Figure 5c, we add calculated CMC for SDS in two other monovalent chloride salts (LiCl and KCl) and one 2:1 salt ($MgCl_2$). The calculated dispersion coefficient for Mg^{2+} is 0.343×10^{-50} J m^3. Like Figure 5a, Figure 5c shows that we can predict the lyotropic series with reasonable quantitative agreement. The dramatic lowering of the CMC in the divalent $MgCl_2$ salt is also

dx.doi.org/10.1021/la501008x | Langmuir 2014, 30, 6373–6383

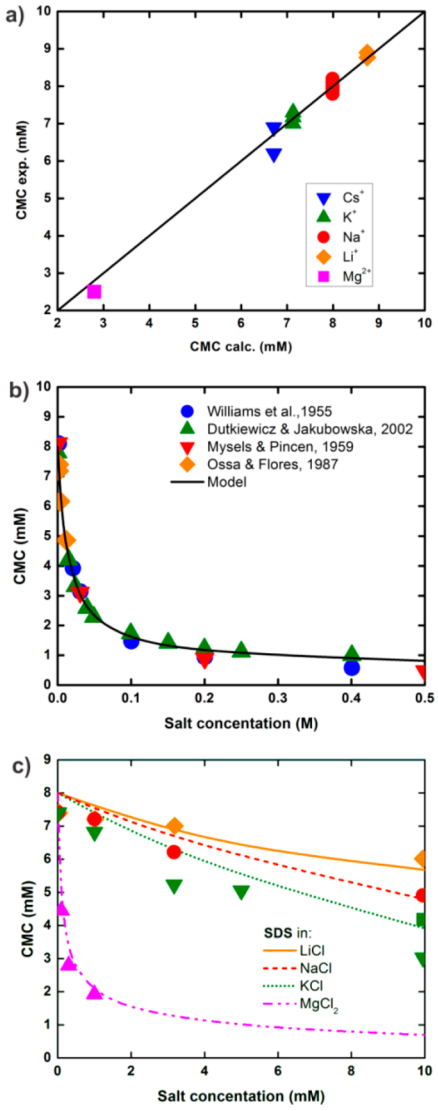

Figure 5. (a) Calculated vs experimental[41−50] CMC of dodecyl sulfates. (b) CMC of SDS as a function of NaCl concentration. The markers are experimental data,[47,50−52] and the solid line is the model prediction. (c) CMC of SDS as a function of chloride salt concentration. The markers are experimental data, and the lines are model predictions: solid line and diamonds[52] for LiCl; dashed line and circles[52] for NaCl; dotted line, green triangles[52] and square[53] for KCl; and dotted-dashed line and purple triangles[54] for $MgCl_2$. All calculations are at 25 °C.

accurately replicated. When dispersion potentials are not taken into account (not shown), we find that ion specificity is virtually lost (all lines collapse into a single line), and the ion-specific variations of the CMC are no longer reproduced by the model. This highlights the vital role that quantum fluctuation forces play in the accurate implementation of ion-specific effects.

B. Molecular Structure of SDS Micelles. There is considerable interest nowadays in exploring the detailed nanostructure of molecular self-assemblies such as micelles. Ion-specific effects can have a dramatic effect on the size and composition of molecular aggregates, and we employ our model to shed light on the mechanisms that govern self-assembly. An analysis of the molecular structure of a micelle can involve several parameters, including aggregation numbers, micellar radius, degree of ion binding at the micelle surface of charge, counterion density profiles in the double layer around the micelle, micelle surface potential, and so forth. In general, these attributes are difficult to determine experimentally, and the error in experiments may be much higher than that in CMC measurements. Theoretical models such as the one presented in this article can potentially be useful in filling in the gaps in experimental data.

Figure 6 shows the predicted aggregation numbers for SDS micelles in NaCl and LiCl salts. Our calculated aggregation

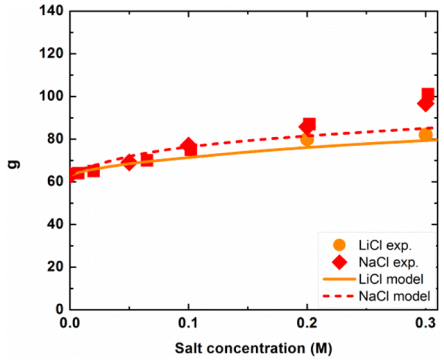

Figure 6. Aggregation numbers for SDS micelles in salts as a function of salt concentration. Markers, experiment;[42,55,56] lines, theory.

number for SDS in water (without salt) is 63 molecules, matching the experimental data well. The well-established trend that the aggregation number increases with salt concentration is captured as well, and so is the lyotropic series (not shown), with micelle size increasing as the counterion is varied from Li^+ to Na^+, K^+, Cs^+, and Mg^{2+}. At higher salt concentration, the agreement with experiment for NaCl slightly deteriorates, most probably due to changes in the micellar shape that are not captured in the theory. In our model, we consider only spherical and globular micelles and do not include the sphere-to-rod transition.

The degrees of counterion binding onto SDS micelles for four different monovalent salts are shown in Figure 7a. The role of β_i in the free energy of micellization is complex, as it affects the steric repulsions through the ionic hydrated radii (Li > Na) and the interface formation energy through the bare ionic radii (Li < Na). The solid lines in Figure 7a indicate the total counterion binding, the dotted lines, the binding of Na^+ ions dissociated from surfactant heads, and the dashed lines, the binding of salt counterions. We see that the binding of kosmotropic ions, such as Na and Li, increases, while the binding of chaotropic ions such as K and Cs, decreases with salt concentration. The predicted degrees of counterion binding are significantly lower than in experimental data. One reason may be that in practice there is no unambiguous distinction between bound and free counterions, and there is no well-defined transition point between the two. Thus, it is not surprising that data on counterion binding in different types of studies varies widely.

Perhaps a more informative feature of the system is the counterion density profiles in the double layer around the micelles. The calculated counterion profiles for four different salts (at c = 0.3 M) are shown in Figure 7b. In general, without dispersion forces, the counterion concentration as a function of the distance from the micelle surface shows a gradual decrease with no well-defined transition point, and the profiles for

dx.doi.org/10.1021/la501008x | Langmuir 2014, 30, 6373−6383

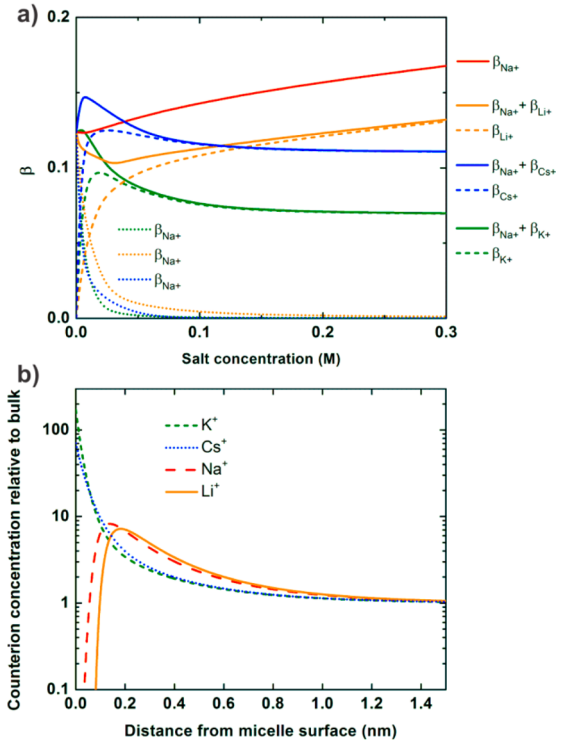

Figure 7. (a) Degree of counterion binding onto SDS micelles as a function of salt concentration at 25 °C. (b) Ion-specific concentration profiles relative to the bulk for four different alkali counterions as a function of distance from the micellar surface.

different monovalent ions are the same (no ion specificity). The profiles change drastically when dispersion potentials are included. We see that for the chaotropic ions (K^+, Cs^+), which experience an attractive dispersion potential with the surface, there is a significant increase in the concentration close to the micelle surface and a corresponding depletion away from it.

In contrast, for the kosmotropic ions (Li^+, Na^+) which experience a repulsive dispersion potential, we see significant depletion very close to the micelle surface (within 1 Å of it) and accumulation slightly further away from it. Figure 7b clearly demonstrates the importance of dispersion forces and why externally imposed Stern layers or distances of closest approach are not needed when dispersion interactions are included. These distances are automatically taken into account through the counterion concentration profiles. We see that K^+ and Cs^+ can get very close to the surface and reach all the way to the surface of charge, whereas Li^+ and Na^+ have a distance of closest approach, slightly closer for Na (less kosmotropic) and slightly further from the micelle surface for Li (more kosmotropic).

We can also integrate the ion concentration profiles to calculate the fraction of bound charge. The fraction of bound charge per headgroup, equal to the surface adsorption excess near the micelle surface, is given by

$$\beta = \frac{4\pi}{g}\int_{R_{ch}}^{\infty} dr\, r^2(c_+ + c_- - 2c) \tag{33}$$

where c_+ and c_- are the counterion/co-ion concentrations and c is the bulk concentration. When we calculate β for Na^+ using eq 33, we obtain a value of 0.65 which is in good agreement with the experimental values.

Finally, following the approach of Srinivasan and Blankschtein, we compare our calculated values for the surface potential of SDS micelles with published experimental results obtained from spectroscopic measurements of acid–base indicators (pK_a probes) that reside at the micelle–water interface (Figure 8).

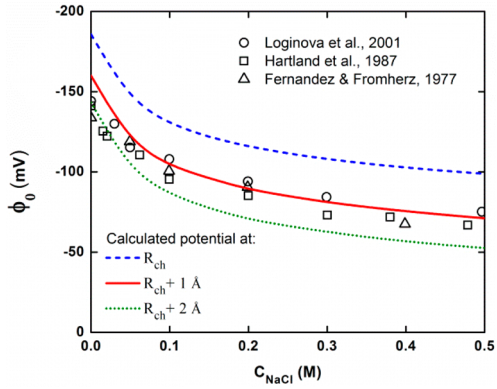

Figure 8. Comparison between the predicted and experimental[56−58] micelle surface electrostatic potential, ϕ_0, for SDS micelles at 25 °C and at an SDS concentration of 10 mM as a function of NaCl concentration. The predicted potentials are for the micelle surface of charge at R_{ch} (blue dashed line), 1 Å from it (solid red line) and 2 Å from it (dotted green line).

The pK_a value of the acid–base indicators is related to the mean electrostatic potential at their site, which is conventionally taken to be at the plane of the surfactant heads. In reality, the acid–base indicators may reside further from the micelle surface depending on whether they have a distance of closest approach, much like the kosmotropic ions in Figure 7b. To this effect, we have also plotted the predicted micelle surface potentials 1 and 2 Å from the surface of charge in Figure 8. As evident from the figure, we find that the calculated value at the surface of charge slightly overestimates the surface potential, while the predicted values 2 Å from the interface slightly underestimate the surface potential. The calculated potential at 1 Å, however, is in agreement with experimental data. The ϕ_0 decrease with salt concentration due to the screening of surface charges is also captured well.

The fact that the acid–base indicators may reside at a distance of about 1 Å from the micelle surface of charge is supported by glancing back at the Na^+ density profile in Figure 7b. We notice that the Na^+ counterions start to accumulate in the double layer about 1 Å away from the micelle surface of charge. We find it reasonable to expect that the acid–base indicators may not penetrate any further than the screening layer of Na^+ counterions. Regardless, the micelle surface potential is captured well both qualitatively and quantitatively. This result indicates that the electrostatic effects associated with micelle formation are quantified accurately by the modified Poisson–Boltzmann theory (with dispersion forces), lending credence to the validity of our model.

IV. CONCLUSIONS

We have presented a molecular thermodynamic theory of micellization for ionic surfactants with added mono- and divalent electrolytes. We incorporate the work of Ninham and co-workers to demonstrate that dispersion forces play a vital role in the aggregation of ionic surfactants and can account for various specific ion effects without the need for externally

dx.doi.org/10.1021/la501008x | Langmuir 2014, 30, 6373−6383

imposed constraints. Our model is predictive and does not have adjustable parameters. We have shown that the concept of chaotropic and kosmotropic ionic behavior, previously accounted for primarily through empirical parameters, now emerges naturally and powerfully through the calculations of ionic polarizabilities and dispersion coefficients with the micelle−water interface. The counterion distribution profiles depicted in Figure 7b are in line with Collins's concept of matching water affinities and automatically incorporate distances of closest approach to the micelle surface into the theory. Our calculations illustrate the fact that ion-specific behavior is integrally dependent on the interacting parts of the interface, macromolecules, and counterions.

The model is validated by comparing our theoretical predictions for the CMC, the micelle molecular structure, and the micelle surface electrostatic potential with the available experimental data. Our results show better agreement with experiment than previous theories, with no adjustable parameters in our model. Stern layers and other ion-surface interaction constraints are not imposed, resulting in a simpler theoretical approach. All of this highlights the vital role of the previously neglected dispersion forces in the molecular thermodynamic modeling of micellization. Our results for the CMC of SDS and other dodecyl sulfates successfully reproduce the lyotropic series and CMC variations with salt concentration. The molecular properties of micelles, such as aggregation numbers and surface potential, are also in agreement with the literature data. In future work, we plan to apply the theory developed here to include other ionic surfactants, investigate the effect of temperature on various micelle parameters, and include the sphere-to-rod transition and correlation effects in order to study the role of higher salt concentrations on the aggregation of surfactants and macromolecules in general.

■ ASSOCIATED CONTENT

Supporting Information

Expressions and derivations for the various free-energy contributions to micelle formation. This material is available free of charge via the Internet at http://pubs.acs.org.

■ AUTHOR INFORMATION

Corresponding Author

*E-mail: abbas.firoozabadi@yale.edu.

Notes

The authors declare no competing financial interest.

■ ACKNOWLEDGMENTS

We are grateful to Livia Moreira for her input in developing the initial stages of the model and Felipe Jiménez for many helpful discussions. We thank the member companies of the Reservoir Engineering Research Institute (RERI) in Palo Alto, CA, for their financial support.

■ REFERENCES

(1) Cacace, M. G.; Landau, E. M.; Ramsden, J. J. The Hofmeister Series: Salt and Solvent Effects on Interfacial Phenomena. *Q. Rev. Biophys.* **1997**, *30*, 241−277.

(2) Hess, B.; van der Vegt, N. F. A. Cation Specific Binding with Protein Surface Charges. *Proc. Natl. Acad. Sci. U.S.A.* **2009**, *106*, 13296−13300.

(3) Knipping, E. M.; Lakin, M. J.; Foster, K. L.; Jungwirth, P.; Tobias, D. J.; Gerber, R. B.; Dabdub, D.; Finlayson-Pitts, B. J. Experiments and Simulations of Ion-Enhanced Interfacial Chemistry on Aqueous NaCl Aerosols. *Science* **2000**, *288*, 301−306.

(4) Shcherbina, A. Y.; Talley, L. D.; Rudnick, D. L. Direct Observations of North Pacific Ventilation: Brine Rejection in the Okhotsk Sea. *Science* **2003**, *302*, 1952−1955.

(5) Tavares, F. W.; Bratko, D.; Prausnitz, J. M. The Role of Salt-Macroion van der Waals Interactions in the Colloid-Colloid Potential of Mean Force. *Curr. Opin. Colloid Interface Sci.* **2004**, *9*, 81−86.

(6) Gradzielski, M. Investigations of the Dynamics of Morphological Transitions in Amphiphilic Systems. *Curr. Opin. Colloid Interface Sci.* **2004**, *9*, 256−263.

(7) Bohmer, M. R.; Koopal, L. K.; Lyklema, J. Micellization of Ionic Surfactants − Calculations Based on a Self-Consistent Field Lattice Model. *J. Phys. Chem.* **1991**, *95*, 9569−9578.

(8) Shelley, J.; Watanabe, K.; Klein, M. L. Simulation of a Sodium Dodecylsulfate Micelle in Aqueous Solution. *Int. J. Quantum Chem.* **1990**, *17*, 103−117.

(9) Bruce, C. D.; Berkowitz, M. L.; Perera, L.; Forbes, M. D. E. Molecular Dynamics Simulation of Sodium Dodecyl Sulfate Micelle in Water: Micellar Structural Characteristics and Counterion Distribution. *J. Phys. Chem. B* **2002**, *106*, 3788−3793.

(10) Sammalkorpi, M.; Karttunen, M.; Haataja, M. Structural Properties of Ionic Detergent Aggregates: A Large-Scale Molecular Dynamics Study of Sodium Dodecyl Sulfate. *J. Phys. Chem. B* **2007**, *111*, 11722−11733.

(11) Mukerjee, P. The Nature of the Association Equilibria and Hydrophobic Bonding in Aqueous Solutions of Association Colloids. *Adv. Colloid Interface Sci.* **1967**, *1*, 241−275.

(12) Hofmeister, F. Zur Lehre von der Wirkung der Salze. Zweite Mittheilung. *Arch. Exp. Pathol. Pharmakol.* **1888**, *24*, 247.

(13) Parsons, D. F.; Boström, M.; Lo Nostro, P.; Ninham, B. W. Hofmeister Effects: Interplay of Hydration, Nonelectrostatic Potentials, and Ion Size. *Phys. Chem. Chem. Phys.* **2011**, *13*, 12352.

(14) Collins, K. D. Ions From the Hofmeister Series and Osmolytes: Effects on Proteins in Solution and in the Crystallization Process. *Methods* **2004**, *34*, 300−311.

(15) Nightingale, E. R., Jr. Phenomenological Theory of Ion Solvation. Effective Radii of Hydrated Ions. *J. Phys. Chem.* **1959**, *63*, 1381−1387.

(16) Dill, K. A.; Bromberg, S. *Molecular Driving Forces*; Garland Science: New York, 2011.

(17) Fennell, C. J.; Bizjak, A.; Vlachy, V.; Dill, K. A. Ion Pairing in Molecular Simulations of Aqueous Alkali Halide Solutions. *J. Phys. Chem. B* **2009**, *113*, 6782−6791.

(18) Boström, M.; Williams, D. R. M.; Ninham, B. W. Specific Ion Effects: Why DLVO Theory Fails for Biology and Colloid Systems. *Phys. Rev. Lett.* **2001**, *87*, 168103.

(19) Boström, M.; Williams, D. R. M.; Ninham, B. W. Surface Tension of Electrolytes: Specific Ion Effects Explained by Dispersion Forces. *Langmuir* **2001**, *17*, 4475−4478.

(20) Parsons, D. F.; Ninham, B. W. Charge Reversal of Surfaces in Divalent Electrolytes: The Role of Ionic Dispersion Interactions. *Langmuir* **2010**, *26*, 6430−6436.

(21) Boström, M.; Williams, D. R. M.; Ninham, B. W. Ion Specificity of Micelles Explained by Ionic Dispersion Forces. *Langmuir* **2002**, *18*, 6010−6014.

(22) Ninham, B. W.; Yaminsky, V. Ion Binding and Ion Specificity: The Hofmeister Effect and Onsager and Lifshitz Theories. *Langmuir* **1997**, *13*, 2097−2108.

(23) Nagarajan, R.; Ruckenstein, E. Theory of Surfactant Self -Assembly: A Predictive Molecular Thermodynamic Approach. *Langmuir* **1991**, *7*, 2934−2969.

(24) Srinivasan, V.; Blankschtein, D. Effect of Counterion Binding on Micellar Solution Behavior: 1. Molecular-Thermodynamic Theory of Micellization of Ionic Surfactants. *Langmuir* **2003**, *19*, 9932−9945.

(25) Srinivasan, V.; Blankschtein, D. Effect of Counterion Binding on Micellar Solution Behavior: 2. Prediction of Micellar Solution Properties of Ionic Surfactant-Electrolyte Systems. *Langmuir* **2003**, *19*, 9946−9961.

(26) Moreira, L.; Firoozabadi, A. Molecular Thermodynamic Modeling of Specific Ion Effects on Micellization of Ionic Surfactants. *Langmuir* **2010**, *26*, 15177−15191.
(27) Koroleva, S. V.; Victorov, A. Modeling of the Effects of Ion Specificity on the Onset and Growth of Ionic Micelles in Solution of Simple Salts. *Langmuir* **2014**, *30*, 3387−3396.
(28) Nagarajan, R. *Theory of Micelle Formation*; CRC Press: Boca Raton, FL, 2003.
(29) Zhou, J. L.; Tits, A. L.; Lawrence, C. T. *User's Guide for FFSQP Version 3.7: A FORTRAN Code for Solving Constrained Nonlinear (Minimax) Optimization Problems, Generating Iterates Satisfying All Inequality and Linear Constraints*; Electrical Engineering Dept and Institute for Systems Research, University of Maryland: College Park, MD, 1997.
(30) Parsons, D. F.; Ninham, B. W. Ab Initio Molar Volumes and Gaussian Radii. *J. Phys. Chem. A* **2009**, *113*, 1141−1150.
(31) Derjaguin, B. On the Repulsive Forces Between Charged Colloid Particles and on the Theory of Slow Coagulation and Stability of Lyophobe Sols. *Trans. Faraday Soc.* **1940**, *35*, 203−215.
(32) Verwey, E. J. W.; Overbeek, J. T. G. *Theory of Stability of Lyophilic Colloids*; Elsevier: New York, 1948.
(33) Mahanty, J.; Ninham, B. W. Self-Energy in Adsorption. *Faraday Discuss. Chem.* **1975**, *59*, 13−21.
(34) Parsons, D. F.; Ninham, B. W. Importance of Accurate Dynamic Polarizabilities for the Ionic Dispersion Interactions of Alkali Halides. *Langmuir* **2010**, *26*, 1816−1823.
(35) Boström, M.; Ninham, B. W. Dispersion Self-Free Energies and Interaction Free Energies of Finite-Sized Ions in Salt Solutions. *Langmuir* **2004**, *20*, 7569−7574.
(36) Landau, L. D.; Lifshitz, E. M. *Electrodynamics of Continuous Media*; Pergamon Press: Oxford, U.K., 1960.
(37) Tavares, F. W.; Bratko, D.; Blanch, H. W.; Prausnitz, J. M. Ion-Specific Effects in the Colloid-Colloid or Protein-Protein Potential of Mean Force: Role of Salt-Macroion van der Waals Interactions. *J. Phys. Chem. B* **2004**, *108*, 9228−9235.
(38) Parsegian, V. A.; Ninham, B. W. Application of the Lifshitz Theory to the Calculation of Van der Waals Forces across Thin Lipid Films. *Nature* **1969**, *224*, 1197−1198.
(39) Ederth, T. Computation of Lifshitz-van der Waals Forces between Alkylthiol Monolayers on Gold Films. *Langmuir* **2001**, *17*, 3329−3340.
(40) Ruckenstein, E.; Nagarajan, R. On Critical Concentrations in Micellar Solutions. *J. Colloid Interface Sci.* **1976**, *57*, 388−390.
(41) Avdeev, M.; Garamus, V.; Rosta, L.; Smirnova, I.; Smirnova, N. SANS Study of Micelle Formation in Aqueous Mixed Solutions of Sodium and Magnesium Dodecylsulfates: Part I. *Physica B* **2000**, *276*−*278*, 339−340.
(42) Bendedouch, D.; Chen, S.-H.; Koehler, W. C. Determination of Interparticle Structure Factors in Ionic Micellar Solutions by Small Angle Neutron Scattering. *J. Phys. Chem.* **1983**, *87*, 2621−2628.
(43) Mukerjee, P.; Mysels, K.; Kapauan, P. Counterion Specificity in the Formation of Ionic Micelles − Size, Hydration, and Hydrophobic Bonding Effects. *J. Phys. Chem.* **1967**, *71*, 4166−4175.
(44) Goddard, E. D.; Harva, O.; Jones, T. G. The Effect of Univalent Cations on the Critical Micelle Concentration of Sodium Dodecyl Sulphate. *Trans. Faraday Soc.* **1953**, *49*, 980−984.
(45) Benrraou, M.; Bales, B. L.; Zana, R. Effect of the Nature of the Counterion on the Properties of Anionic Surfactants. 1. Cmc, Ionization Degree at the Cmc and Aggregation Number of Micelles of Sodium, Cesium, Tetramethylammonium, Tetraethylammonium, Tetrapropylammonium, and Tetrabutylammonium Dodecyl Sulfates. *J. Phys. Chem. B* **2003**, *107*, 13432−13440.
(46) Benton, D. P.; Sparks, B. D. Adsorption from Aqueous Solutions of Ionic Surface-Active Agents by Gold. *Trans. Faraday Soc.* **1966**, *62*, 3244−3252.
(47) Dutkiewicz, E.; Jakubowska, A. Effect of Electrolytes on the Physicochemical Behaviour of Sodium Dodecyl Sulphate Micelles. *Colloid Polym. Sci.* **2002**, *280*, 1009−1014.
(48) Emerson, M. F.; Holtzer, A. On the Ionic Strength Dependence of Micelle Number. II. *J. Phys. Chem.* **1967**, *71*, 1898−1907.
(49) Kim, D.-H.; Oh, S.-G.; Cho, C.-G. Effects of Cs and Na Ions on the Interfacial Properties of Dodecyl Sulfate solutions. *Colloid Polym. Sci.* **2001**, *279*, 39−45.
(50) Williams, R. J.; Phillips, J. N.; Mysels, K. J. The Critical Micelle Concentration of Sodium Lauryl Sulphate at 25° C. *Trans. Faraday Soc.* **1955**, *51*, 728−737.
(51) Mysels, K. J.; Princen, L. H. Light Scattering by Some Lauryl Sulfate Solutions. *J. Phys. Chem.* **1959**, *63*, 1696−1700.
(52) de la Ossa, E. M.; Flores, V. *Tenside Surfact. Det.* **1987**, *24*, 38−41.
(53) Maiti, K.; Mitra, D.; Guha, S.; Moulik, S. P. Salt effect on self-aggregation of sodium dodecylsulfate (SDS) and tetradecyltrimethylammonium bromide (TTAB): Physicochemical correlation and assessment in the light of Hofmeister (lyotropic) effect. *J. Mol. Liq.* **2009**, *146*, 44−51.
(54) Stellner, K. L.; Scamehorn, J. F. Hardness Tolerance of Anionic Surfactant Solutions. 1.Anionic Surfactant with Added Monovalent Electrolyte. *Langmuir* **1989**, *5*, 70−77.
(55) Berr, S. S.; Jones, R. R. M. Effect of Added Sodium and Lithium Chlorides on Intermicellar Interactions and Micellar Size of Aqueous Dodecyl Sulfate Aggregates As Determined by Small-Angle Neutron Scattering. *Langmuir* **1988**, *4*, 1247−1251.
(56) Hartland, G. V.; Grieser, F.; White, L. R. Surface Potential Measurements in Pentanol-Sodium Dodecyl Sulphate Micelles. *J. Chem. Soc., Faraday Trans. 1* **1987**, *83*, 591−613.
(57) Loginova, L. P.; Samokhina, L. V.; Mchedlov-Petrossyan, N. O.; Alekseeva, V. I.; Savvina, L. P. Modification of the Properties of NaDS Micellar Solutions by Adding Electrolytes and Non-Electrolytes: Investigations with Decyl Eosin as a pK_a-Probe. *Colloids Surf., A* **2001**, *193*, 207−219.
(58) Fernandez, M. S.; Fromherz, P. Lipoid pH Indicators as Probes of Electrical Potential and Polarity in Micelles. *J. Phys. Chem.* **1977**, *81*, 1755−1761.